Draft version September 26, 2011
Preprint typeset using LaTeX style emulateapj v. 5/2/11

A TYPE IA SUPERNOVA AT REDSHIFT 1.55 IN THE INFRARED FROM THE CANDELS HUBBLE SPACE TELESCOPE TREASURY PROGRAM

Steven A. Rodney[1], Adam G. Riess[1,2], Tomas Dahlen[2], Louis-Gregory Strolger[3], Henry C. Ferguson[2], Jens Hjorth[4], Teddy F. Frederiksen[4], Benjamin J. Weiner[5], Bahram Mobasher[6], Stefano Casertano[2], David O. Jones[1], Peter Challis[7], S. M. Faber[8], Alexei V. Filippenko[9], Peter Garnavich[10], Or Graur[11], Norman A. Grogin[2], Brian Hayden[10], Saurabh W. Jha[12], Robert P. Kirshner[7], Dale Kocevski[8], Anton Koekemoer[2], Curtis McCully[12], Brandon Patel[12], Abhijith Rajan[2], and Claudia Scarlata[14]

Draft version September 26, 2011

ABSTRACT

We report the discovery of a Type Ia supernova (SN Ia) at redshift $z = 1.55$ with the infrared detector of the Wide Field Camera 3 (WFC3-IR) on the *Hubble Space Telescope (HST)*. This object was discovered in CANDELS imaging data of the Hubble Ultra Deep Field, and followed as part of the CANDELS+CLASH Supernova project, comprising the SN search components from those two *HST* multi-cycle treasury programs. This is the highest redshift SN Ia with direct spectroscopic evidence for classification. It is also the first SN Ia at $z > 1$ found in the infrared and the first with a full rest-frame optical light curve. The classification and redshift are securely defined from a combination of multi-band and multi-epoch photometry of the SN, ground-based spectroscopy of the host galaxy, and WFC3-IR grism spectroscopy of both the SN and host. This object is the first of a projected sample at $z > 1.5$ that will be discovered by the CANDELS and CLASH programs. The full CANDELS+CLASH SN Ia sample will enable unique tests for evolutionary effects that could arise due to differences in SN Ia progenitor systems as a function of redshift. This high-z sample will also allow measurement of the SN Ia rate out to $z \approx 2$, providing a complementary constraint on SN Ia progenitor models.

Subject headings: supernovae: general

1. INTRODUCTION

In their use as "standardizable" candles, Type Ia supernovae (SN Ia) have become one of the pillars of modern observational cosmology. SN Ia provided the first direct evidence for an accelerating expansion of the Universe (Riess et al. 1998; Perlmutter et al. 1999), an effect now commonly attributed to "dark energy." The present challenge for SN Ia cosmology is to understand the dark energy equation-of-state parameter, $w = P/(\rho c^2)$ (Turner & White 1997; Caldwell et al. 1998; Garnavich et al. 1998). Recent surveys have targeted SN Ia in one of three broad redshift (z) categories, illustrated in Figure 1 as follows.

1. Low-z: SN Ia in the low-redshift regime ($0.02 \lesssim z \lesssim 0.1$) provide the anchor for the SN Ia Hubble diagram (Jha et al. 2006; Hicken et al. 2009; Contreras et al. 2010). These "local" SNe have been used to develop empirical tools for using light curve shapes to classify high-z SNe and measure their luminosities.

2. Mid-z: At intermediate redshifts ($0.1 \lesssim z \lesssim 1$) ground-based surveys such as ESSENCE, SDSS, and SNLS[14] have built up samples of hundreds of SN Ia, testing models that assume a constant dark energy equation-of-state parameter, w_0 (Wood-Vasey et al. 2007; Kessler et al. 2009a; Sullivan et al. 2011). Current and future programs such as PTF, Pan-STARRS, and LSST[15] will bridge both of these regimes, providing unified samples with thousands of SN Ia to $z \approx 0.8$.

3. High-z: The high-redshift range ($0.8 \lesssim z \lesssim 1.5$) has been populated almost exclusively by the *Hubble Space Telescope (HST)* with optical surveys using the Advanced Camera for Surveys (ACS) (Riess et al. 2004; Riess et al. 2007; Suzuki et al. 2011). These high-redshift objects reach back to the era of deceleration, enabling tests of models with a time-varying dark-energy component $w(z)$ and checks against extreme SN Ia systematics. From the set of high-z SN Ia with measured light curves, the highest redshift on record is SN 1997ff at $z \approx 1.7$ (Riess et al. 2001). This object was found in a passive host with an old stellar population, strongly suggesting

[1] Department of Physics and Astronomy, The Johns Hopkins University, Baltimore, MD 21218.
[2] Space Telescope Science Institute, Baltimore, MD 21218.
[3] Department of Physics, Western Kentucky University, Bowling Green, KY 42101.
[4] Dark Cosmology Centre, Niels Bohr Institute, University of Copenhagen, Juliane Maries Vej 30, DK-2100 Copenhagen, Denmark.
[5] Department of Astronomy, University of Arizona, Tucson, AZ 85721.
[6] Department of Physics and Astronomy, University of California, Riverside, CA 92521.
[7] Harvard/Smithsonian Center for Astrophysics, Cambridge, MA 02138.
[8] Department of Astronomy and Astrophysics, University of California, Santa Cruz, CA 92064.
[9] Department of Astronomy, University of California, Berkeley, CA 94720-3411.
[10] Department of Physics, University of Notre Dame, Notre Dame, IN 46556.
[11] Department of Astrophysics, Tel Aviv University, 69978 Tel Aviv, Israel.
[12] Department of Physics and Astronomy, Rutgers, The State University of New Jersey, Piscataway, NJ 08854.
[14] Department of Astronomy, University of Minnesota, 116 Church Street SE, Minneapolis, MN 55455, USA.

[14] ESSENCE: Equation of State: SupErNovae trace Cosmic Expansion; SDSS: Sloan Digital Sky Survey; SNLS: SuperNova Legacy Survey.
[15] PTF: the Palomar Transient Factory; Pan-STARRS: the Panoramic Survey Telescope And Rapid Response System; LSST: the Large Synoptic Survey Telescope.

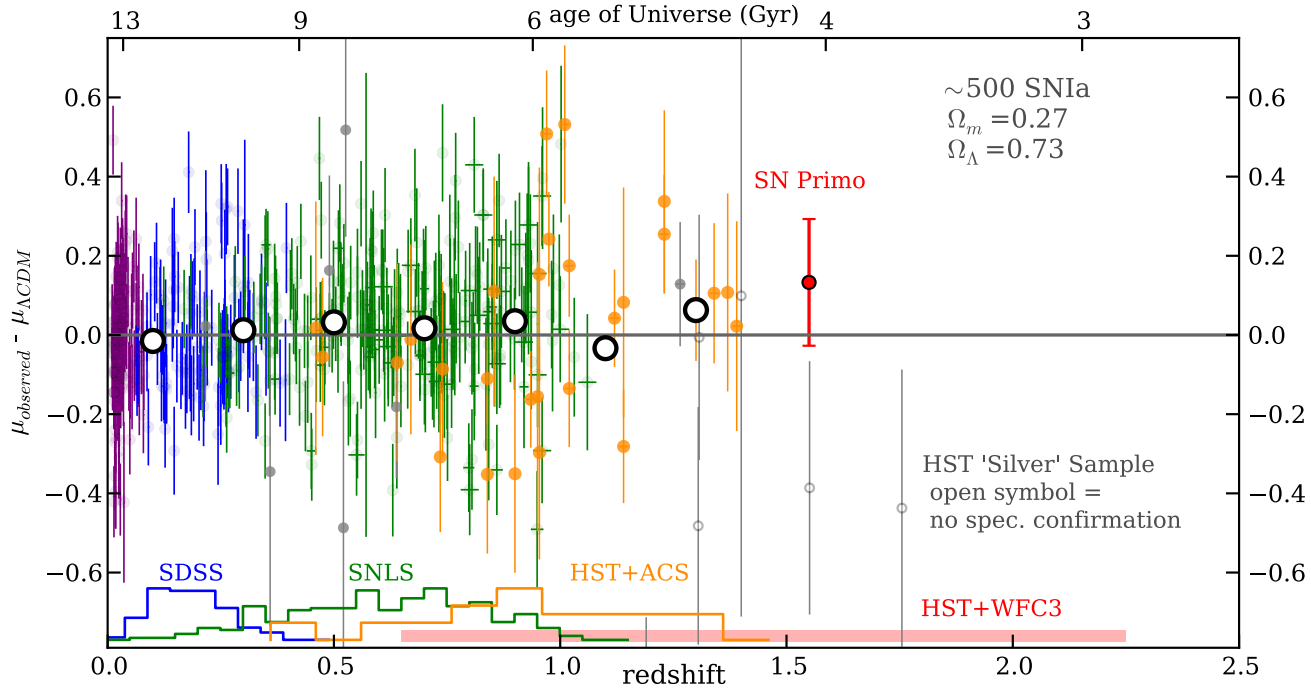

Figure 1. SN Ia Hubble residuals diagram, plotting distance modulus relative to the ΛCDM cosmology versus redshift. Colored points with error bars show the compilation of ∼ 500 SN Ia from Conley et al. (2011): the low-z sample in purple and the mid-z SNe in blue and green, with large open circles showing the mean values in redshift bins of width 0.2. For the high-z range, the "Gold" and "Silver" SN Ia samples from Riess et al. (2007) and Riess et al. (2004) are shown in gold and grey points, respectively, with open symbols indicating objects that lack a spectroscopic classification. Separately normalized histograms along the lower edge show the distribution of points for each survey, and the red bar shows the expected reach of the *HST* MCT survey presented in this work.

it is a SNIa. However, there is no reliable spectroscopic measurement of the SN, it has only a sparsely observed light curve, and the host redshift relies on a photo-z and a questionable single-line detection. More and better observations are clearly needed before any inferences about the high-z SN Ia population can be drawn.

Collectively, the SN Ia samples out to $z \approx 1.5$ are consistent with a description of dark energy as the cosmological constant, $w(z) = -1$ (Riess et al. 2007; Hicken et al. 2009; Sullivan et al. 2011; Suzuki et al. 2011). Figure 1 shows a recent collection of ∼ 500 SN Ia from Conley et al. (2011), with distances plotted relative to the best-fit ΛCDM cosmology. Histograms on the lower edge show the redshift range of each contributing survey. With the addition of the Wide Field Camera 3 infrared detector (WFC3-IR) on *HST*, a new window has been opened, allowing the detection of SN Ia at $z > 1.5$. This very high redshift regime provides an excellent laboratory in which to test for possible evolution of the SN Ia population (Riess & Livio 2006).

The ratio of dark energy to matter density (now ∼ 2.7) decreases with redshift as $\rho_\Lambda/\rho_M \propto (1+z)^{3w} \propto (1+z)^{-3}$ (e.g., Turner & White 1997), so the $z > 1.5$ Universe is matter dominated. The solid curves in Figure 2 show two scenarios for variable dark energy that are consistent with current observations (e.g., Sullivan et al. 2011). Parameterizing $w = w_0 + w_a(1+a)$, we can see that changes in the dark-energy parameters w_0 and w_a would change the observed SN Ia magnitudes at $z > 1.5$ by less than 0.1 mag. This means that a larger deviation in the peak magnitudes of these supernovae from those seen nearby would provide evidence for evolution of the SN Ia population.

Riess & Livio (2006) considered SN Ia progenitor models that predict a decrease in the observed SN Ia luminosity for objects with a higher initial progenitor mass, due to changes in the internal C/O ratio at the time of explosion (Domínguez et al. 2001; Hoeflich et al. 1998). If such an effect exists, then we might expect to see its signature becoming apparent in the SN Ia population at $z > 1.5$. The green curve in Figure 2 shows a somewhat crude realization of this model, under the assumption that SN Ia progenitors require 2.5 Gyr of post-main-sequence (MS) binary evolution before reaching the point of explosion. The blue curve plots the same model, but with the assumption of 0.4 Gyr of post-MS evolution. These two assumptions provide rough bounds on the plausible range of progenitor evolution timescales. Both curves are marked with points indicating the minimum possible progenitor mass for a SN Ia exploding at that redshift: low-mass progenitor stars cannot evolve through their MS lifetime plus a long binary mass-transfer stage in time to explode and be observed as a $z > 1.5$ SN Ia. The illustrative Domínguez et al. (2001) model suggests that this systematic shift toward higher mass progenitors could result in an observable shift in the mean SN Ia magnitude at high redshift.

The high-z SN Ia sample also provides an important constraint on progenitor models through the measurement of SN Ia rates. Binary stellar population synthesis combined with models of SN Ia explosion conditions can provide a prediction for the delay-time distribution

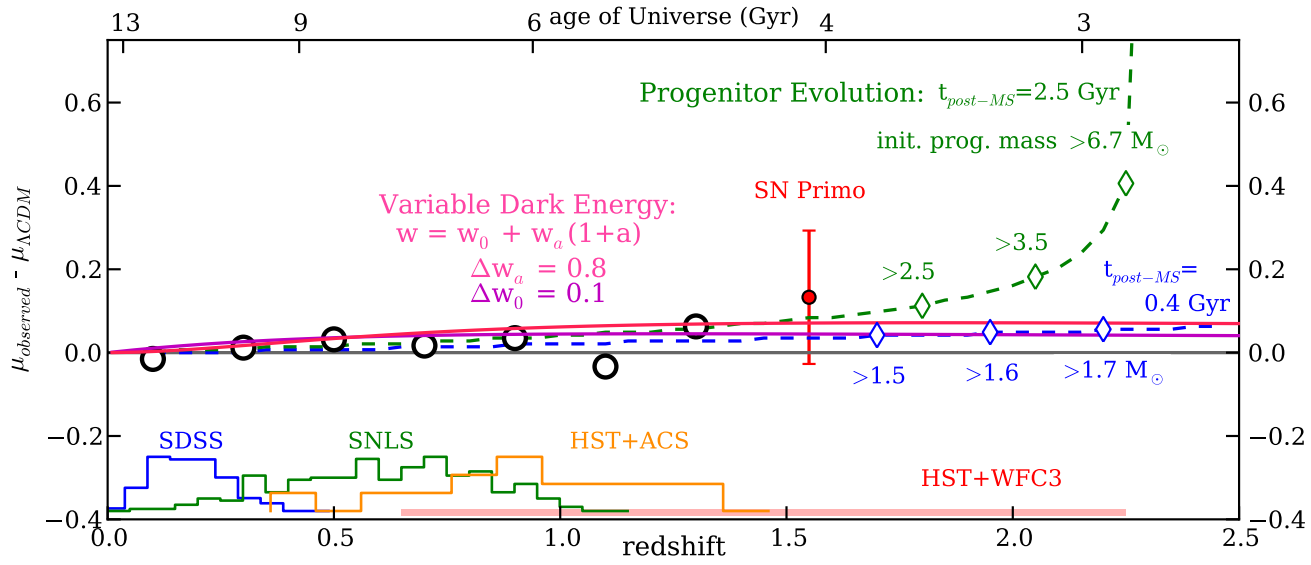

Figure 2. SN Ia Hubble residuals diagram, as in Figure 1, now without the background points for individual SNe. Solid curves in pink and purple depict the effects of a variable dark energy that can be parameterized as $w = w_0 + w_a(1 + a)$. Green and blue dashed curves show two realizations of a model that predicts systematic changes in the mean apparent magnitude of high-z SN Ia; see Domínguez et al. (2001) and Riess & Livio (2006) for details. The green curve assumes that SN Ia require a post-main-sequence (MS) evolution timescale of 2.5 Gyr, so that low-mass progenitors with long MS lifetimes will not have enough time to reach explosion at $z > 1.5$. Under this assumption, the minimum progenitor mass increases significantly with redshift, as indicated by the labeled diamonds along the curve. The blue curve shows the same model, but with an assumed post-MS evolution time of 0.4 Gyr.

(DTD) that should be observed for the SN Ia progenitor population at any redshift. Convolving this predicted DTD with measurements of the cosmic star formation rate produces a prediction for the SN Ia rate as a function of redshift. There is general consensus on the measured SN Ia rate out to $z \approx 1$, and these observations can be well matched by a number of progenitor models (see, e.g., Graur et al. 2011, hereafter G11, for a recent compilation). It is at $z > 1$ that the SN Ia rate starts to be strongly dependent on the shape of the DTD, and the few measurements in this regime have so far placed only modest constraints on possible progenitor models (Strolger et al. 2004; Kuznetsova et al. 2008; Dahlen et al. 2008, hereafter D08; G11). The WFC3-IR survey described in this work will provide a significant improvement in the high-z SN Ia rate measurements by substantially increasing the spectroscopically confirmed SN Ia sample at $z > 1$.

Metallicity effects should be more pronounced in the $z > 1.5$ SN Ia sample, and may be apparent in the observed SN Ia rates. Consider a SN Ia progenitor system with a long delay time of ~ 3 Gyr. For this object to be observed at $z \approx 2$, the formation redshift would have been $z \approx 10$, close to the redshift of reionization (Komatsu et al. 2011) when the Universe was *only* ~ 300 Myr old. This long-delay SN would have been born in the first generation of stars, in an extremely metal-poor environment. The progenitor model of Hachisu et al. (1996) invokes a metal-driven wind from the accreting white dwarf, and therefore requires a high metallicity as a prerequisite for SN Ia explosion. If this progenitor track accounts for a significant fraction of the SN Ia population, then the Hachisu et al. (1996) model would suggest that the observed SN Ia rate may be much lower at $z > 1.5$ than otherwise expected.

In this work we present an early result from the CANDELS+CLASH Supernova project (PI: Riess). This search-and-follow SN program is a composite survey combining the SN search components from two MCT programs, both of which were designed with cadence and filter choices that enable the detection of high-z SNe using the WFC3-IR detector. The Cosmic Assembly Near-infrared Deep Extragalactic Legacy Survey (CANDELS, PI: Faber & Ferguson) is a wide-field survey targeting five famous fields (GOODS-S, GOODS-N, COSMOS, EGS, and UDS). Observations and data processing for CANDELS are described by Grogin et al. (2011) and Koekemoer et al. (2011), respectively. The second MCT program is the Cluster Lensing And Supernova survey with Hubble (CLASH, PI: Postman), which is targeting 25 low-redshift galaxy clusters (Postman et al. 2011). The SNe contributing to the high-redshift SN Ia sample from CLASH will be located behind the clusters in the primary fields, or in the extended survey area provided by *HST* parallel observations. Both programs will span three years, from 2010 to 2013.

Within the first epoch of CANDELS imaging, the SN team discovered a high-z SN candidate, dubbed SN Primo. As described below, this object was later confirmed as a SN Ia at $z = 1.55$, making it the highest redshift SN Ia with a spectroscopic confirmation. The detection and follow-up observations of SN Primo are detailed in §2, and in §3 we explore the potential for this survey to extend the SN Ia sample to $z \approx 2$.

2. SN Primo

SN Primo was found in CANDELS search images of the GOODS-S field collected on 2010 October 10 (UT dates are used throughout this paper). It was detected in both WFC3-IR search filters (F125W = J and F160W = H) as well as the broad "white light" filter of WFC3-UVIS (F350LP = W); see Grogin et al. (2011) for a com-

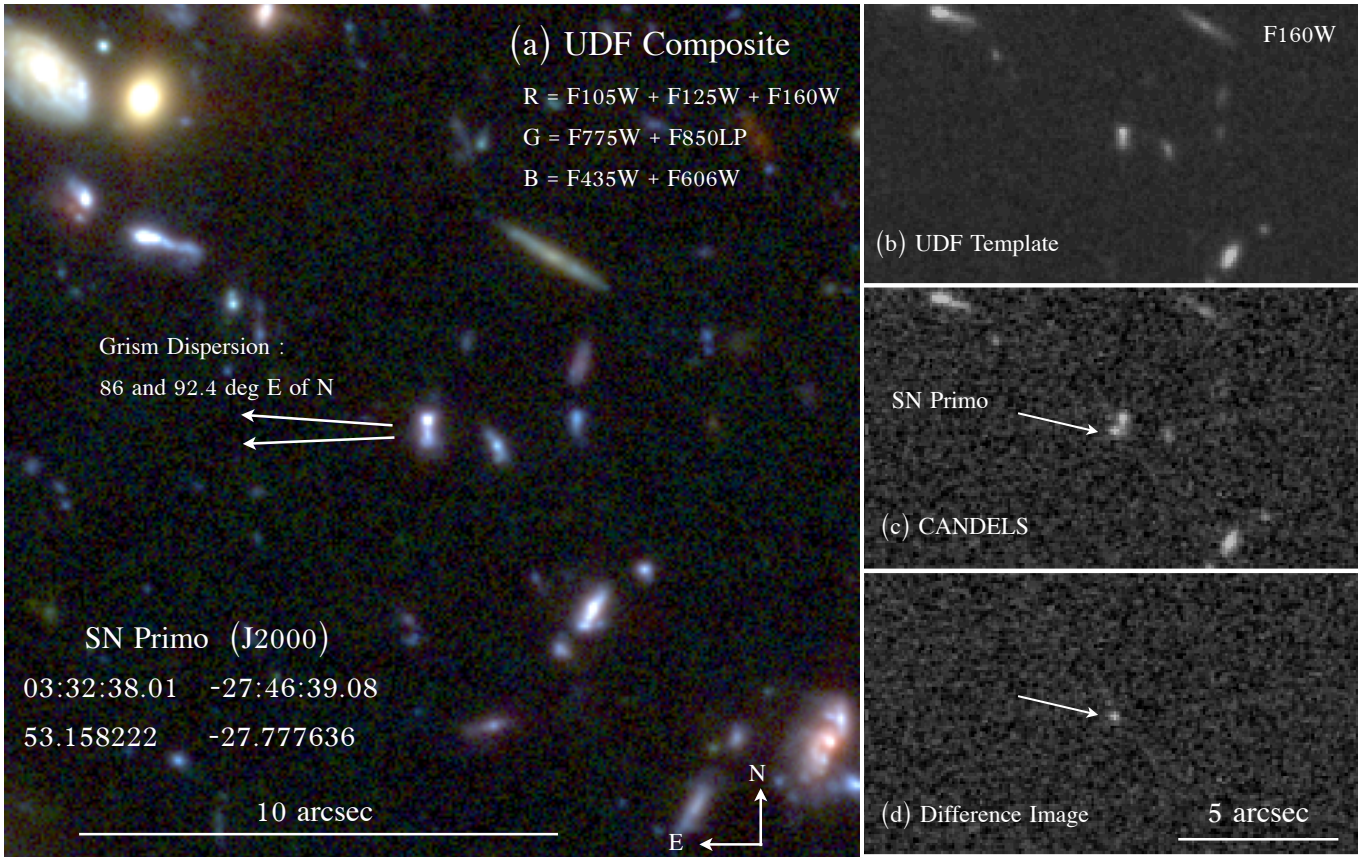

Figure 3. (a) Composite image of the SN Primo host galaxy and surroundings in the UDF. (b) The F160W (H) template image, from UDF data. (c) CANDELS search-epoch image in F160W, from 2010 October 26. (d) F160W difference image (c−b), showing SN Primo near peak brightness.

plete description of the CANDELS observations. The use of F350LP to discriminate core-collapse SNe (CC SNe) from SN Ia is presented in §2.1. It was located within the 11.5 arcmin^2 Hubble Ultra Deep Field (HUDF) region, which had been recently observed using WFC3-IR under a Cycle 17 *HST* program (GO-11563, PI: Illingworth). SN Primo was found in a search by eye of difference images that were constructed by subtracting a deep template HUDF image from the October 10 CANDELS images, as shown in Figure 3.[16]

Upon discovery, the magnitudes and colors of SN Primo were found to be consistent with a SN Ia at $z > 1$ (§2.1). The host-galaxy photo-z was estimated at $z_{\rm phot} = 1.56$ (§2.2). These observations gave us an early indication that this object was very likely to be a SN Ia, so we triggered target of opportunity follow-up observations from the ground with the Very Large Telescope (VLT) and from space with *HST*. The VLT observations (Frederiksen et al. 2011, in prep) confirmed the redshift of the host galaxy (§2.2), and the *HST* observations built up the infrared (IR) light curve (§2.3) and also provided a grism spectrum of both the SN and its host galaxy (§2.4).

[16] The discovery of SN Primo was indeed serendipitous: Without pre-existing WFC3-IR data to serve as a template, 90% of the GOODS-S field could not be searched for SNe on 10 Oct, 2010. It was only the lucky circumstance of appearing in the HUDF that enabled SN Primo to be discovered.

2.1. *Color*

A key improvement for the CANDELS and CLASH programs over past *HST* SN surveys is the availability of the F350LP filter on the WFC3-UVIS camera. This very broad "white light" filter transmits all optical light, and is therefore extremely efficient. In an exposure of just 400 s we can reach a signal-to-noise ratio (S/N) of 20 for point sources as faint as Vega magnitude 25.4. For a SN at $z = 1.5$ the F350LP filter samples the rest-frame ultraviolet, blueward of 3600 Å, offering a stark contrast between mostly blue CC SNe and much redder SN Ia.

The ideal scenario for SN classification is to include F350LP observations within the same *HST* visit as our primary near-IR search images in F125W (J) and F160W (H). Competing requirements from the static-sky science goals of CANDELS sometimes prevent this optimal arrangement, in which case we use the F606W (V) filter on ACS in an overlapping visit taken within 3 days.

After discovery in the CANDELS imaging data, SN Primo was recovered in prior F160W observations from *HST* program GO-11563 taken in September, 2010, putting a tight constraint on the explosion date and rise time. With the date of peak brightness well-defined, the F350LP−F160W color-magnitude measurement from the discovery epoch provides an important early classification indicator, as shown in Figure 4. Using the known redshift of the host galaxy (§2.2), we use the SNANA simulation tools (Kessler et al. 2009b) to

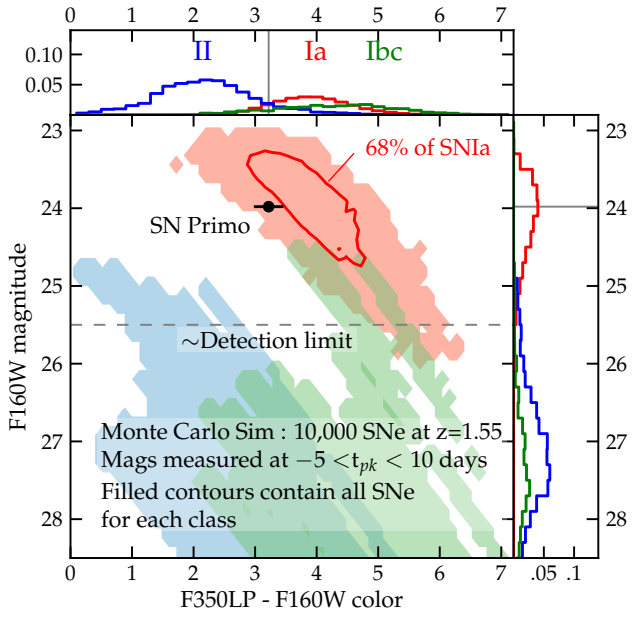

Figure 4. Color-magnitude diagram showing the F350LP−F160W color diagnostic, used in the initial identification of SN Primo as a high-z SN Ia candidate. The SNANA light curve simulator (Kessler et al. 2009b) was used to generate 10,000 SNe at $z = 1.55$, with colors and magnitudes measured at times between 5 days before and 10 days after peak brightness, in the observer frame. Relative frequencies for each subclass were drawn from Li et al. (2011) (24% Ia, 19% Ibc, 57% II) and luminosity functions follow Richardson et al. (2002), Kiewe et al. (2010), and Drout et al. (2010). The shaded contours and corresponding histograms show the full extent of each SN subclass (i.e., they contain 100% of the simulated objects for each class). Type II SNe are shown in blue, Type Ibc in green, and Type Ia in red. The solid red line in the central figure demarcates the region containing 68% of the simulated SN Ia. The SN Ia simulation uses a parameterized model based on the SALT2 light curve fitter (Guy et al. 2007). CC SNe are simulated using 44 spectrophotometric templates that are based on well-observed low-z CC SNe (hence the appearance of stripes and gaps in the CC SN contours).

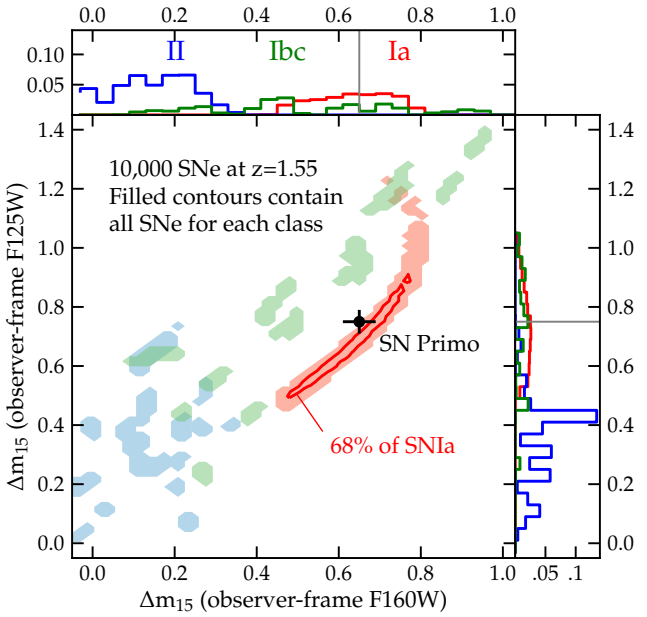

Figure 5. The light curve width parameter Δm_{15} for the same simulated SNe shown in Fig. 4. The Δm_{15} parameter measures the increase in observed magnitude from the peak to 15 rest-frame days after peak, and is tightly correlated with absolute magnitude for SN Ia (Phillips 1993). For each simulated SN we measure Δm_{15} in both F125W (J) and F160W (H), and plot contours containing the entire sample in the main panel (blue for Type II, green for Type Ibc, and red for Type Ia). Histograms of the one-dimensional projections are shown in the top and side panels. As in Fig. 4, the CC SN contours show spotty coverage of the parameter space, because they are based on 44 discrete templates, rather than a single extensible light curve model as used for the SN Ia.

generate 10,000 simulated SNe of Types Ia, Ibc, and II. The CC SN simulation is limited by the dearth of well-measured light curve templates at low redshift. Whereas the SN Ia simulation is defined by a parameterized model with strong empirical constraints, our simulated CC SNe are based on just 44 low-z templates. This deficiency is reflected in the patchy and streaky CC SN contours in both Figure 4 and 5. Nevertheless, the SNANA simulation provides the most complete picture of the CC SN population that is possible without extrapolation.

The observed F350LP−F160W color for SN Primo at peak brightness is consistent with a Type Ia SN at $z = 1.55$, but could also be matched by CC SN templates at that redshift. The F160W (H) magnitude is more difficult to reconcile with a core-collapse model. One does not want to use a strong prior on the apparent magnitude of high-z SNe as the basis for classification, as cosmological effects could have an impact on observed magnitudes. However, SN Primo is observed at a full 2 mag brighter than the brightest Type II SN of similar color. The less common Type Ib/c SNe come closer to matching SN Primo's F160W magnitude, but only in the case of the very rare overluminous SNe Ibc, of which only a handful are known at low redshift.

Thus, SN Primo's position on the color-magnitude diagram provides good evidence for an initial classification as a SN Ia. After making this assessment, follow-up observations were then executed to fill out the IR light curve and measure the SN spectrum, providing further diagnostics to confirm or refute this classification.

2.2. *Host Galaxy*

Immediately after discovery, the photometric redshift (photo-z) of a SN host galaxy is one of the most important tools for segregating targets of interest from impostor transients (e.g., active galactic nuclei, CC SNe at lower redshifts, etc.). The probability distribution of the photo-z for SN Primo's host is sharply peaked at $z = 1.56$ by the extremely deep existing *HST* data in the HUDF, with a 68% confidence range of $1.51 < z < 1.64$ and a 95% confidence range $1.45 < z < 1.76$. The principal constraint comes from the offset between optical photometry and IR photometry, since the 4000 Å break falls between the optical and IR at $z \approx 1.5$. This emphasizes the importance of accurate IR photometry for determining the host galaxy photo-z at $z > 1.5$.

Although SN Primo itself was too faint for ground-based follow-up spectroscopy, the host galaxy was accessible. A VLT observation using the X-Shooter spectrograph (D'Odorico et al. 2006) detected strong emission lines from Hα, [O III], and [O II]. These lines fixed the redshift of the host with exquisite precision

to z=1.54992±0.00007, and also confirmed the initial photometric classification of the host as a strongly star-forming galaxy. A complete discussion of the VLT observations and the SN Primo host galaxy will be presented by Frederiksen et al. (2011, in prep).

2.3. *Photometry*

As detailed in Table 1, the fading light curve was followed from 2010 November through 2011 January, with 6 visits from the SN follow-up program and 2 return visits from CANDELS. The light curve is plotted in Figure 6 with the best-fitting template (SN 2005cf), as determined by the SOFT light curve classification program (Rodney & Tonry 2009, 2010). Reinforcing the color classification, we find that this best-fitting light curve template is a normal SNIa at the redshift of the host galaxy (SN 2005cf has a light curve width of $\Delta m_{15}(B) = 1.05 \pm 0.03$ mag). The SOFT fit with various SN Ia light curve templates can allow for $0 < A_V < 0.5$ mag of host-galaxy extinction. Using the MLCS2k2 light curve fitter (Jha et al. 2007), we find similarly undistinguished fit parameters: a very normal light curve shape parameter $\Delta = -0.12 \pm 0.10$ and a host-galaxy extinction of $A_V = 0.14 \pm 0.14$. These estimates of low A_V are supported by the VLT spectrum of the host, in which the emission lines are consistent with no reddening (Frederiksen et al. 2011, in prep).

The light curve shape measurement provides a strong test of the SN Ia classification, as shown in Figure 5. The Δm_{15} parameter quantifies the shape of a SN Ia light curve as the change in magnitude from peak to 15 rest-frame days past maximum (Phillips 1993). For SN Ia this parameter varies over a small range and is well correlated across adjacent photometric bands. Figure 5 shows that SN Primo's light curve shape is consistent with the narrow band defined by our simulated SN Ia at $z = 1.55$.

The patchy CC SN contours in Figure 5 do not reflect the true range of CC SN light curve shapes, due to the incomplete information available for modeling this population (see discussion in §2.1). Thus, one cannot rule out the possibility that SN Primo's position in Δm_{15} parameter space is consistent with a Type Ibc population that is underrepresented by the SNANA templates. The available information, however, lends strong support to the initial classification as a SN Ia.

2.4. *Grism*

In the first epoch of follow-up observations, SN Primo was observed using the WFC3 G141 grism (resolution $R \approx 130$, 1100–1700 nm). Observations were executed in three visits spaced over 7 days,[17] for a total integration time of 21.7 ks (see Table 1). SN Primo was separated from the nucleus of its host galaxy by $\sim 0.5''$(0.23″E, 0.44″S), so it was possible to select the orientation to minimize contamination of the SN spectrum by its own host. These grism data were processed using the aXe software package,[18] and the spectra for SN Primo and its host were separately extracted.

[17] The initial observing plan would have completed the grism observations in a single day, but a guiding error resulted in a failure during the second visit, so it had to be rescheduled for the subsequent week.

[18] http://axe.stsci.edu

Table 1
SN Primo Photometric Data

UT Date	MJD	Filter	Exp.Time	Vega Mag
2010 Oct 10.9*	55479.9	F350LP	434	27.2±0.2
2010 Aug 06.9	55414.9	F125W	11023	>28.0
2010 Oct 10.9*	55479.9	F125W	1006	24.37±0.05
2010 Nov 01.4	55501.4	F125W	406	24.48±0.06
2010 Nov 07.7	55507.7	F125W	1306	24.57±0.03
2010 Nov 21.2	55521.2	F125W	2512	24.94±0.04
2010 Nov 28.4	55528.4	F125W	1006	25.03±0.07
2010 Dec 05.2	55535.2	F125W	2512	25.62±0.07
2010 Dec 13.8	55543.8	F125W	5123	25.83±0.06
2011 Jan 17.7	55578.7	F125W	1006	27.00±0.40
2011 Mar 05.6	55625.6	F125W	1006	>27.2
2010 Aug 08.4	55416.4	F160W	11024	>27.0
2010 Sep 02.9	55441.9	F160W	10824	>26.2
2010 Sep 14.9	55453.9	F160W	5512	25.39±0.15
2010 Oct 10.9*	55479.9	F160W	1056	23.98±0.04
2010 Oct 26.6	55495.6	F160W	1206	24.27±0.05
2010 Nov 07.7	55507.7	F160W	1306	24.53±0.08
2010 Nov 22.9	55522.9	F160W	2512	24.61±0.06
2010 Nov 28.4	55528.4	F160W	956	24.57±0.11
2010 Dec 05.3	55535.3	F160W	2512	24.88±0.14
2011 Jan 17.7	55578.7	F160W	1106	25.72±0.19
2011 Mar 05.6	55625.6	F160W	1106	>26.2
2010 Oct 26.7	55495.7	G141	6618	(grism obs)
2010 Nov 01.5	55501.5	G141	15036	(grism obs)

* Date of discovery

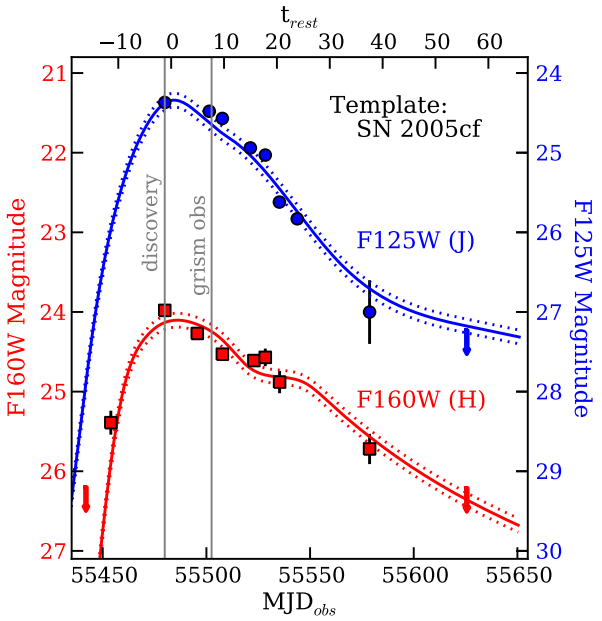

Figure 6. The SN Primo light curve for F125W (J) as blue circles and F160W (H) as red squares. Solid lines show the best-fitting template, as determined by the SOFT light curve classification program, and dashed lines indicate the model uncertainty (see Rodney & Tonry 2009). The best-fit template is based on the light curve of the normal Type Ia SN 2005cf (Wang et al. 2009).

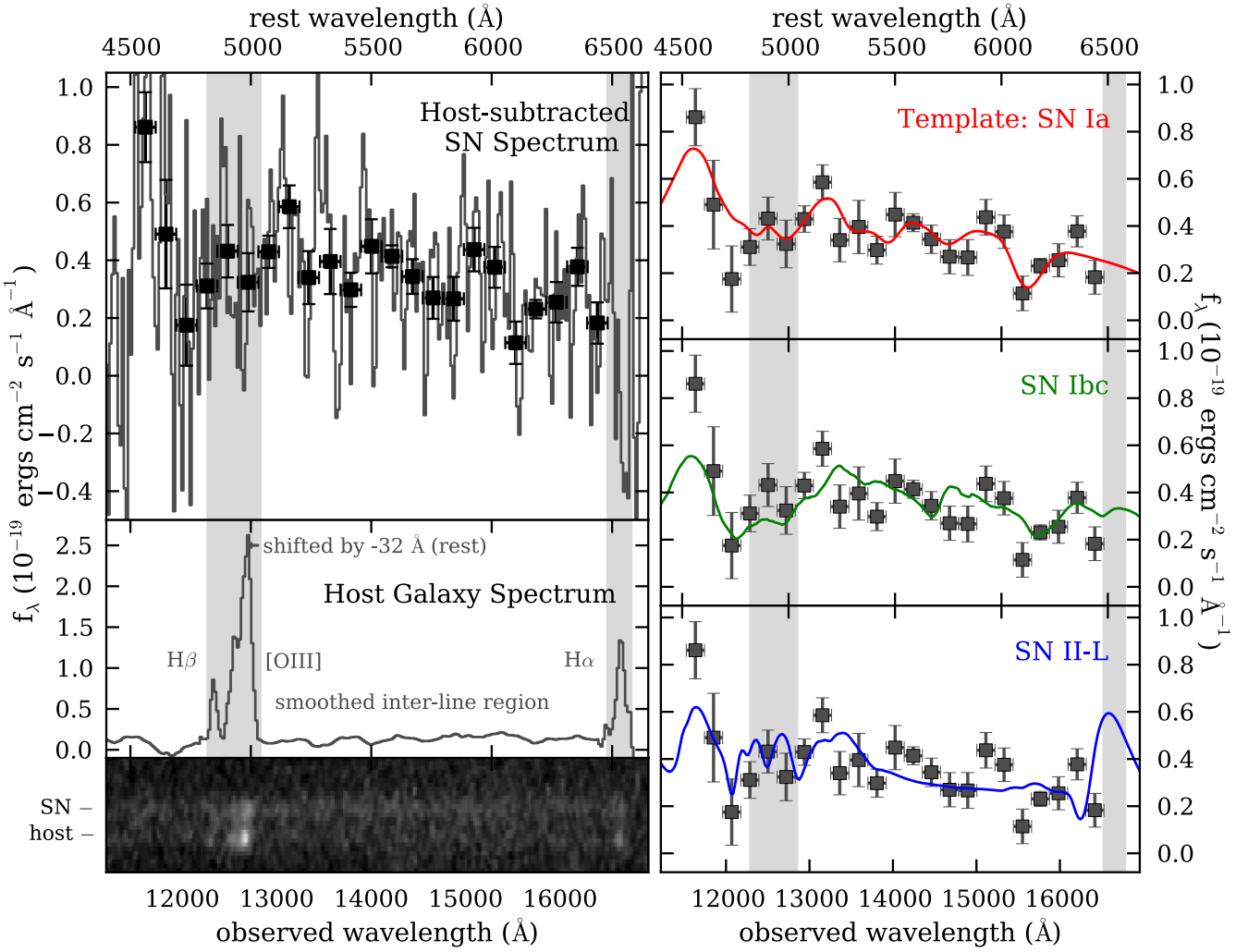

Figure 7. The HST G141 grism spectrum of SN Primo. The left side depicts the spectral data reduction process: the bottom panel shows the 2-D grism spectrum, the center panel shows the host-galaxy spectrum, smoothed and shifted as described in the text, and the top panel shows the host-subtracted SN spectrum. Grey lines show the unbinned spectrum in rest wavelength for the known redshift $z = 1.55$. Solid points show the average value after 2σ clipping in 80 Å bins. On the right side, the same binned points are shown in each of the three panels, with three template spectra overlaid as solid lines for SNe of Type Ia, Ibc, and II. All templates are depicted for the known age of the SN at the time of the grism observation: 6 rest-frame days past peak brightness. The vertical grey bands indicate regions where the SN spectrum was contaminated by bright emission lines from the host galaxy: Hβ and [O III] on the blue side, and Hα on the red side.

The two-dimensional (2D) grism trace is shown in the bottom-left panel of Figure 7, in which the bright emission knots from Hβ, [O III], and Hα are readily apparent. These emission lines also contaminate the spectrum extracted at the location of SN Primo, visible as the distinct upper trace. To remove the host component from the SN Primo spectrum, we smoothed the nuclear host spectrum in the regions between emission lines while leaving the lines untouched (center-left panel of Figure 7). As can be seen in Figure 3c, SN Primo was offset to the E of its host by 0.23″. In the slitless grism observations, this spatial separation along the dispersion direction is translated into a wavelength separation between the SN features and the superimposed host-galaxy features. To correct for this offset, the smoothed host spectrum was shifted by −32 Å in the rest frame. We then scaled the flux of the entire host spectrum so that the emission lines match the lines in the SN Primo spectrum. This smoothed, shifted, and scaled host spectrum was subtracted from the SN Primo spectrum to get an isolated SN spectrum. Finally, we deredden the SN spectrum for a host galaxy extinction of $A_V = 0.3$ mag, $R_V = 3.1$, consistent with the range of extinctions that produce acceptable SOFT and MLCS2k2 fits (§2.3). Alternate assumptions for host A_V in the range [0,0.5] do not alter our conclusions. For template fitting, the host-subtracted spectrum was binned into wavelength bins of width 80 Å with iterative 2σ clipping. This binned spectrum is plotted over the unbinned SN spectrum in the top-left panel of Figure 7.

The SN Primo spectrum is noisy, and spans only $\sim$ 2000 Å in rest wavelength, which would make it challenging to classify without any additional information. However, with the redshift tightly constrained to $z = 1.55$ and the age of the SN at time of observation narrowly defined by the light curve, the only degrees of freedom for spectral template matching are the choice of template and the flux scaling. The SN Primo spectrum, shows a

broad trough from 4600 to 5100 Å (in rest wavelength), and a narrower drop starting at ~ 6100 Å. The former is roughly consistent with the Fe/Si/S complex and the latter is a good match to Si II λ6355 — both characteristic features of a normal SN Ia spectrum. These features can also be found in SN Ib/c spectra shortly after maximum, although they are typically less pronounced than in SN Ia (Filippenko 1997).

The right side of Figure 7 shows best-fitting spectral templates from the three principal SN classes: Ia, Ib/c, and II. The best match for the SN Primo spectrum is the SN Ia template drawn from the Hsiao et al. (2007) model, with $\chi^2/\nu = 21.3/18 = 1.2$. The SN Ibc template from the Nugent template library[19] is a poorer fit, with $\chi^2/\nu = 44.7/18 = 2.5$. The best-fitting SN II template (also from the Nugent set) is worse still, at $\chi^2/\nu = 63.1/18 = 3.5$. The grism spectrum therefore provides a final confirmation of the SN Primo classification as a SN Ia.

3. DISCUSSION

The discovery and confirmation of SN Primo demonstrates the new capability of *HST* to both detect and follow SN Ia at redshifts above 1.5 using the WFC3 IR detector. Given the depth of our survey observations in the IR, we are able to detect a normal SN Ia like SN Primo to redshifts as high as $z \approx 2.3$, where it would appear with an unreddened peak (Vega) magnitude around F125W = 25.3 and F160W = 25.1 mag with a S/N of 10 (i.e., uncertainties of 0.1 mag).

After detecting SNe at $z \approx 2$, however, the real challenge lies in the follow-up campaign. The classification of SN Primo as a SN Ia is built on four layers of evidence. First, the F350LP−F160W color and the host-galaxy photometric redshift suggest that the object may be a high-z SN Ia (Figure 4). Second, ground-based follow-up spectra from the VLT pin down the redshift, narrowing the range of possible models and strengthening the SN Ia case. Third, in Figure 5 a well-sampled light curve defines SN Primo's position in the Δm_{15} parameter space as consistent with the narrow SN Ia band. Finally, the spectrum shown in Figure 7 reveals SN Ia spectral features that confirm the SN Ia classification.

This complete array of classification indicators will not always be possible, especially for SNe at the highest redshifts. For example, a SN that lies close to the core of a bright host galaxy is a very challenging grism target. Conversely, an object in a low surface brightness host galaxy may have a very poorly determined redshift. In some cases the SN age at discovery is not well defined, reducing the precision of the color-magnitude classification tools. Each SN and host presents a unique set of circumstances, demanding a uniquely tailored follow-up strategy. In all cases, however, the use of multiple, complementary diagnostics will ensure that the CANDELS+CLASH sample of SN Iaat $z > 1.5$ will have reliable classifications.

As the CANDELS+CLASH SN survey progresses, the first question that the growing $z > 1.5$ SN sample will be able to address is simply, how many SN Ia are there at $z > 1.5$? This rate measurement provides an important constraint on models of SN Ia progenitors through measurement of the DTD. Past *HST* programs using the ACS were able to extend the SN Ia rate measurement to $z \approx 1.5$, but only with very weak statistical constraints (Strolger et al. 2004, D08). The D08 results suggest a decline in the SN Ia rate at $z > 1.2$, but that claim rests on only three SN detections that populate the highest redshift bin. Ground-based rate measurements from the Subaru Deep Field (SDF) survey have claimed a higher SN Ia rate at $z \approx 1.5$ (G11). The SDF results have larger statistical significance (their sample has 10 SN Ia at $z \approx 1.5$, where D08 has 3). However, there is a greater potential for classification errors, as the G11 sample has only single-epoch detections with a one-year interval, no spectroscopic confirmation of the SNe, and no spectroscopic host redshifts above $z = 1.2$.

The CANDELS+CLASH survey will be able to resolve this dispute observationally with two rate measurements. First, in the $1 < z < 1.5$ range, this program is the first SN search to use IR bands for SN discovery, making it less sensitive to dust extinction that could have obscured SNe in optical surveys. Second, this survey will for the first time extend the SN Ia rate measurement to $z \approx 2$. Extrapolating the rate measurements from D08 and G11, we expect to discover ~ 10 SN Ia at $z > 1.5$ over the three-year CANDELS+CLASH program. As with SN Primo, all of these objects will have secure classifications and the best available redshifts.

Finally, the full sample of $z > 1.5$ SNe will enable a direct test for evolution in the properties of SN Ia. In Figures 1 and 2 we see that SN Primo is consistent with the standard ΛCDM model. Figure 6 shows that SN Primo is very well matched by a light curve template based on SN 2005cf, a normal SN Ia with a light curve width of $\Delta m_{15}(B) = 1.05$ mag. The spectral features shown in Figure 7 are also consistent with a normal SN Ia. Thus, SN Primo alone provides no evidence for evolution of the SN Ia population with redshift, but with only a single well-studied object so far one cannot draw any meaningful conclusions. Extending these comparisons to the final sample of ~ 10 high-z SN Ia may provide useful constraints on evolution of the SN Ia population.

Acknowledgments:

We would like to thank our Program Coordinators, Beth Perriello and Tricia Royle, our Contact Scientist Sylvia Baggett, and the entire *Hubble* planning team, for their efforts in support of this challenging program. The WFC3 team has made substantial contributions to the program by calibrating and characterizing the instrument, and have provided much useful advice. We thank David Koo and Asantha Cooray of CANDELS for helpful discussions and review of this paper, and Marc Postman and Larry Bradley of CLASH for their steadfast support of the CLASH SN search program.

Financial support for this work was provided by NASA through grants HST-GO-12060 and HST-GO-12099 from the Space Telescope Science Institute, which is operated by Associated Universities for Research in Astronomy, Inc., under NASA contract NAS 5-26555.

Support for this research at Rutgers University was provided in part by NSF CAREER award AST-0847157 to SWJ.

The Dark Cosmology Centre is supported by the Danish National Research Foundation.

Facilities: HST (WFC3) VLT (X-shooter)

[19] http://supernova.lbl.gov/ñugent/nugent_templates.html .

REFERENCES

Caldwell, R. R., Dave, R., & Steinhardt, P. J. 1998, Physical Review Letters, 80, 1582
Conley, A., et al. 2011, ApJS, 192, 1
Contreras, C., et al. 2010, AJ, 139, 519
Dahlen, T., Strolger, L.-G., & Riess, A. G. 2008, ApJ, 681, 462
D'Odorico, S., et al. 2006, in SPIE Conference Series, Vol. 6269
Domínguez, I., Höflich, P., & Straniero, O. 2001, ApJ, 557, 279
Drout, M. R., et al. 2010, arXiv:1011.4959
Filippenko, A. V. 1997, ARA&A, 35, 309
Garnavich, P. M., et al. 1998, ApJ, 509, 74
Graur, O., et al. 2011, arXiv:1102.0005
Grogin, N. A., et al. 2011, arXiv:1105.3753
Guy, J., et al. 2007, A&A, 466, 11
Hachisu, I., Kato, M., & Nomoto, K. 1996, ApJ, 470, L97+
Hicken, M., et al. 2009, ApJ, 700, 331
Hoeflich, P., Wheeler, J. C., & Thielemann, F. K. 1998, ApJ, 495, 617
Hsiao, E. Y., et al. 2007, ApJ, 663, 1187
Jha, S., et al. 2006, AJ, 131, 527
Jha, S., Riess, A. G., & Kirshner, R. P. 2007, ApJ, 659, 122
Kessler, R., et al. 2009a, ApJS, 185, 32
—. 2009b, PASP, 121, 1028
Kiewe, M., et al. 2010, arXiv:1010.2689
Koekemoer, A. M., et al. 2011, arXiv:1105.3754
Komatsu, E., et al. 2011, ApJS, 192, 18
Kuznetsova, N., et al. 2008, ApJ, 673, 981
Li, W., et al. 2011, MNRAS, 412, 1441
Perlmutter, S., et al. 1999, ApJ, 517, 565
Phillips, M. M. 1993, ApJ, 413, L105
Postman, M., et al. 2011, arXiv:1106.3328
Richardson, D., et al. 2002, AJ, 123, 745
Riess, A. G., et al. 1998, AJ, 116, 1009
Riess, A. G., & Livio, M. 2006, ApJ, 648, 884
Riess, A. G., et al. 2001, ApJ, 560, 49
—. 2007, ApJ, 659, 98
Riess, A. G., et al. 2004, ApJ, 607, 665
Rodney, S. A., & Tonry, J. L. 2009, ApJ, 707, 1064
—. 2010, ApJ, 715, 323
Strolger, L.-G., et al. 2004, ApJ, 613, 200
Sullivan, M., et al. 2011, ApJ, 737, 102
Suzuki, N., et al. 2011, arXiv:1105.3470
Turner, M. S., & White, M. 1997, Phys. Rev. D, 56, 4439
Wang, X., et al. 2009, ApJ, 697, 380
Wood-Vasey, W. M., et al. 2007, ApJ, 666, 694